

## Nuclear size and boundary effects on the fusion barrier of oxygen with carbon

Y. Eyal

*Department of Isotope Research, The Weizmann Institute of Science, Rehovot, Israel*

M. Beckerman,\* R. Chechik, Z. Fraenkel, and H. Stocker†

*Department of Nuclear Physics, The Weizmann Institute of Science, Rehovot, Israel*

(Received 6 October 1975)

Absolute yields, energy spectra, and angular distributions of heavy residual nuclei ranging from Ne to Si have been measured in the reactions  $^{16}\text{O} + ^{12}\text{C}$ ,  $^{17}\text{O} + ^{12}\text{C}$ , and  $^{18}\text{O} + ^{12}\text{C}$ . For each system measurements have been performed at seven beam energies corresponding to the range 7 to 14 MeV c.m. The formation of the above products is shown to be consistent with a reaction which proceeds through the formation and decay of an excited and equilibrated composite system. Systematic differences between the absolute magnitudes of the fusion cross sections of the three reactions have been observed. It is shown that these differences are closely related to the expected differences in the nuclear size and surface diffuseness of the oxygen isotopes. Possible implications for astrophysical processes are briefly discussed.

[ NUCLEAR REACTIONS Complete fusion of  $^{16}\text{O} + ^{12}\text{C}$ ,  $^{17}\text{O} + ^{12}\text{C}$ , and  $^{18}\text{O} + ^{12}\text{C}$  at  $E = 7-14$  MeV c.m. Measured  $\sigma(E, \theta)$  of evaporation residues. Deduced fusion barrier characteristics. ]

### I. INTRODUCTION

Compound nucleus reactions are known to constitute the major fraction of the interactions between complex nuclei at low and moderate bombarding energies. Nevertheless, little information is available on complete fusion cross sections of heavy-ion beams with light target nuclei. Such information is needed for the study of fusion barriers and their dependence on nuclear charges, sizes, and shapes of the interacting nuclei. Other features of heavy-ion complete-fusion reactions which are of interest include limitations on the fusion due to angular momentum effects and the decay properties of the composite system.

In the low energy region, compound nucleus formation cross sections have been measured for the reactions  $^{12}\text{C} + ^{12}\text{C}$  (Ref. 1),  $^{16}\text{O} + ^{12}\text{C}$  (Ref. 2 and 3), and  $^{16}\text{O} + ^{16}\text{O}$  (Ref. 4) at energies from below the Coulomb barrier to slightly above it. The experimental techniques employed included mainly the measurement of emitted light charges particles and  $\gamma$  rays. Interest in these reactions arose from their importance in astrophysical processes. In addition, numerous intensive investigations have been conducted over the last 15 years in order to understand the nature of the structures which appear in the excitation functions of many of the outgoing channels of the reactions  $^{12}\text{C} + ^{12}\text{C}$ ,  $^{16}\text{O} + ^{12}\text{C}$ , and  $^{16}\text{O} + ^{16}\text{O}$ . Lists of relevant publications can be found in Refs. 1-4. It has been shown that all prominent decay channels proceed predominantly through the compound nucleus mechanism.

In this work we describe a study of complete fusion reactions between  $^{16}\text{O}$ ,  $^{17}\text{O}$ , and  $^{18}\text{O}$  projectiles and  $^{12}\text{C}$  nuclei in the energy region 7 to 14 MeV c.m. In the fusion of oxygen with carbon, excited silicon compound nuclei are formed. These compound nuclei decay mainly through emission of light particles, yielding heavy residual nuclei ranging from Ne to Si. The excitation energies which have been reached in the present experiment are indicated in Fig. 1. This figure also includes ground-state  $Q$  values for many of the decay channels. Our measurements involved determination of yields, energy spectra, and angular distributions of the heavy residual nuclei mentioned above. Complete fusion cross sections as a function of bombarding energy have been determined by measuring directly the absolute yields of the heavy residues. The experimental procedure employed in the present work is described briefly in Sec. II. The experimental data are presented in Sec. III. In Sec. IV we concentrate on the decay of the three silicon composite systems. In particular, we study the differential yields of the heavy reaction products and their recoil characteristics. The investigation of these important properties has been ignored in most previous studies of heavy-ion reactions. The complete fusion excitation functions of the reactions  $^{16}\text{O} + ^{12}\text{C}$ ,  $^{17}\text{O} + ^{12}\text{C}$ , and  $^{18}\text{O} + ^{12}\text{C}$  are then analyzed in order to obtain information on the fusion barriers of the corresponding systems. In view of the strong absorption character of heavy-ion collisions, the absolute magnitudes of the fusion cross sections as well as their energy dependence

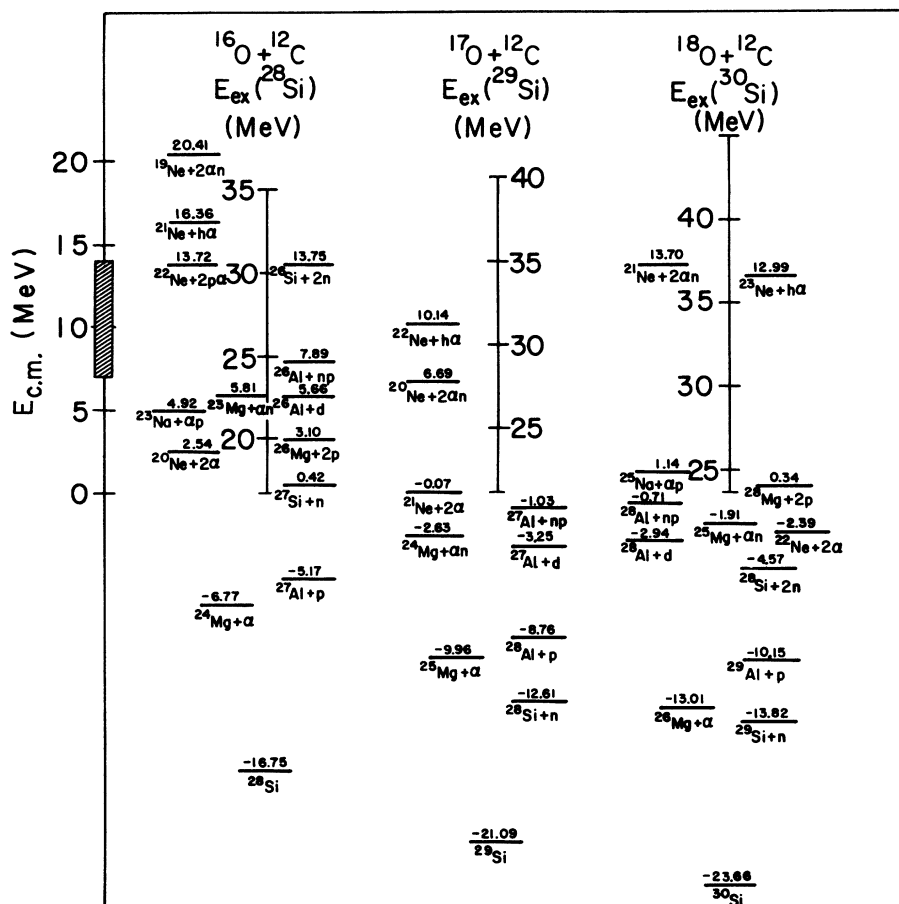


FIG. 1. Ground-state  $Q$  values and excitation energies for the reactions of  $^{16}\text{O}$ ,  $^{17}\text{O}$ , and  $^{18}\text{O}$  with  $^{12}\text{C}$ . (In this figure  $h$  represents  $^3\text{He}$ ).

are expected to depend on the nuclear size and boundary diffuseness of the oxygen isotopes. The underlying idea of this investigation is to resolve the effects of the nuclear interaction from those of the dominant Coulomb repulsion by comparing systems in which the latter interaction is very similar. Section V is devoted to a short summary and conclusions.

## II. EXPERIMENTAL PROCEDURE

Beams of  $^{16}\text{O}$ ,  $^{17}\text{O}$ , and  $^{18}\text{O}$  were provided by the EN tandem Van de Graaff accelerator of the Weizmann Institute of Science, Rehovot. The carbon targets consisted of self-supporting thin ( $2\text{--}20 \mu\text{g}/\text{cm}^2$ ) natural carbon foils ( $98.8\%$   $^{12}\text{C}$ ). Heavy reaction products were detected and identified by two separate  $\Delta E$ - $E$  counter telescopes. In each telescope the  $\Delta E$  detector consisted of a thin gas-flow proportional counter filled with a mixture of 90% argon and 10% methane. The gas pressure was kept constant and was adjusted to provide a  $\Delta E$  detector with a nominal thickness of about  $170 \mu\text{g}$

$/\text{cm}^2$ . Thin thermoplastic films of about  $70 \mu\text{g}/\text{cm}^2$  were used as front windows for the gas counters. The  $E$  detectors, which consisted of solid-state surface barrier detectors, were placed on the internal rear sides of the gas counters. The pulses of the  $\Delta E$  and  $E$  detectors were processed with conventional electronics, and the coincident data were accumulated in a  $64 \times 128$  array within an on-line PDP-9 computer.

The angular acceptance of each counter telescope was about  $0.3^\circ$  in the laboratory frame and subtended a solid angle of about  $6 \times 10^{-5}$  sr at the target. The angular setting for each detector was read directly on a  $360^\circ$  scale with an accuracy better than  $0.1^\circ$ . The dial reading was calibrated by left-right measurements of the elastic scattering. Two small surface barrier detectors were placed in fixed positions in the forward hemisphere of the chamber to serve both as beam and target thickness monitors. To obtain absolute values of the cross sections, the elastic scattering cross sections at forward angles were normalized to calcu-

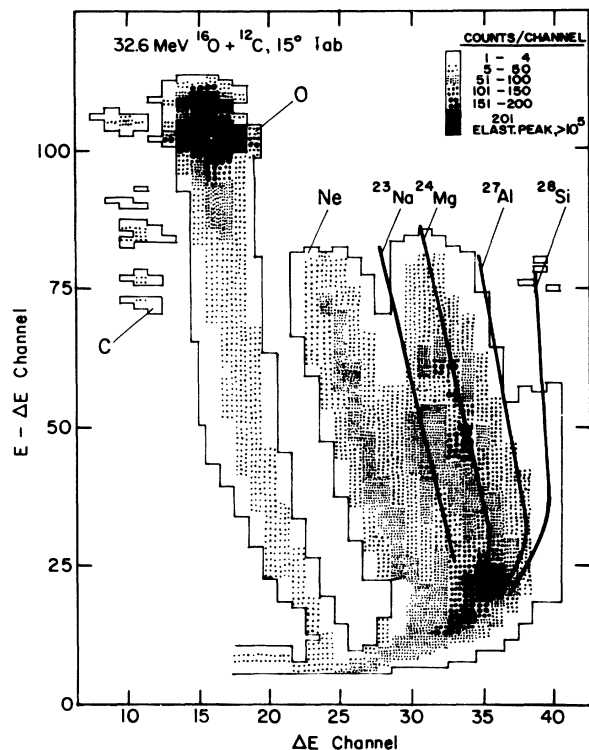


FIG. 2. A  $\Delta E$  vs  $E-\Delta E$  display of heavy reaction products measured in the reaction 32.63 MeV  $^{16}\text{O}$  on  $^{12}\text{C}$  at  $15^\circ$  lab (see text).

lated Rutherford cross sections.

The energy response of the counter telescopes to heavy ions was determined experimentally by detecting F, Na, Mg, Al, Si, and Cl ions recoiling elastically from appropriate thin targets in oxygen bombardments.

Some accumulation of silicon and oxygen contaminants on target during bombardments has been observed. Elastically recoiled Si events were clearly distinguished from the fusion residues. The amount of oxygen in target was determined from the elastic scattering of oxygen on oxygen measured with the aid of the monitor detectors. On the basis of the  $^{16}\text{O}+^{16}\text{O}$  fusion data<sup>4</sup> it is estimated that the upper limit of the contribution of the oxygen contaminant to the measured yield is 3% at 14 MeV c.m. and 0.5% at 7 MeV c.m. The presence of the natural 1.1%  $^{13}\text{C}$  in targets was ignored throughout the analysis.

### III. EXPERIMENTAL RESULTS

An  $E-\Delta E$  vs  $\Delta E$  display of the heavy residual nuclei and their kinetic energy distributions measured at  $15^\circ$  lab in the reaction 32.63 MeV  $^{16}\text{O}$  on

$^{12}\text{C}$  is shown in Fig. 2. The four thick lines marked by  $^{23}\text{Na}$ ,  $^{24}\text{Mg}$ ,  $^{27}\text{Al}$ , and  $^{28}\text{Si}$  indicate the experimentally calibrated loci of the corresponding isotopes. A large yield of neon is clearly observed. Neon nuclei have also been observed in the reactions  $^{17}\text{O}+^{12}\text{C}$  and  $^{18}\text{O}+^{12}\text{C}$ , but their yields were smaller than in the reaction  $^{16}\text{O}+^{12}\text{C}$ . No fluorine events have been detected during the course of the present experiment.

As can be seen in Fig. 2 the energy resolution of the  $\Delta E$  detector was sufficient to resolve completely the elastically scattered nuclei and the fusion residues. However, except for neon, the energy resolution was not sufficient to resolve the various fusion products, although some distinction between them could be made in the high energy part of the spectrum. Since the stopping powers of low energy heavy ions are very close to one another, their signals overlap at very low recoil energies, irrespective of the energy resolution. It is also seen in Fig. 2 that the low energy tail of the elastic scattering peak, caused mainly by slit scattering, interferes slightly with the low energy tail of the fusion products. A low energy cutoff at about 6.5 MeV was therefore imposed on the measurements. However, it was found from experimental systematics, and verified by evaporation calculations, that the portion of the events with energies below the cutoff level was negligible in most cases and always less than 15%. The unmeasured fraction of the fusion products was estimated from the calculations, and the fusion yield was corrected accordingly.

For each system measurements were performed at seven beam energies spanning the region 7 to 14 MeV c.m. Incident and corresponding c.m. energies are listed in Table I. At each bombarding energy, energy spectra and differential cross sections of heavy residual nuclei were measured from  $4^\circ$  to about  $31^\circ$  in the laboratory frame in steps of  $1^\circ$  or  $2^\circ$ . A few double-differential cross sections in the laboratory frame are displayed in Figs. 3 and 4. Due to the insufficient resolution in the  $\Delta E$  dimension, events in the  $E-\Delta E$  dimension were summed over the entire elemental spectrum, except for the data shown in Figs. 4(a) and 4(c), where the neon yield could be resolved from the rest of the fusion residues down to fairly low recoil energies. Since the energy response in the  $E-\Delta E$  coordinate depends on the atomic number (see Fig. 2), the combined energy spectra in Figs. 3, 4(b), and 4(d) should be considered as approximate energy spectra only. The kinetic energy scales were adjusted at each angle to the product which contributes mostly to the yield at that angle. This information was obtained from evaporation calculations. At some angles average (with respect to the atomic

TABLE I. Bombarding energies, c.m. energies, and complete fusion cross sections  $\sigma$  for the reactions of  $^{16}\text{O}$ ,  $^{17}\text{O}$ , and  $^{18}\text{O}$  with  $^{12}\text{C}$ . The energies were corrected for losses in the targets. The uncertainty in the c.m. energy scale is  $^{+0.02}_{-0.04}$  MeV.

Projectile	$E_{\text{lab}}$ (MeV)	$E_{\text{c.m.}}$ (MeV)	$\sigma$ (mb)
$^{16}\text{O}$	16.33	6.99	$13.2 \pm 2.5$
	18.63	7.99	$80.5 \pm 8.4$
	20.99	8.99	$195 \pm 19$
	23.31	9.99	$327 \pm 28$
	27.98	11.99	$540 \pm 46$
	30.03	12.87	$632 \pm 52$
	32.63	13.99	$773 \pm 60$
$^{17}\text{O}$	16.91	7.00	$18.3 \pm 2.9$
	19.28	7.98	$101 \pm 11$
	21.74	8.99	$239 \pm 19$
	24.13	9.99	$409 \pm 30$
	28.98	11.99	$597 \pm 42$
	31.11	12.87	$661 \pm 49$
	33.84	14.00	$751 \pm 57$
$^{18}\text{O}$	17.48	6.99	$25.2 \pm 3.0$
	19.98	7.99	$123 \pm 10$
	22.48	8.99	$299 \pm 23$
	24.98	9.99	$418 \pm 31$
	29.98	11.99	$652 \pm 46$
	32.18	12.87	$724 \pm 63$
	34.98	13.99	$794 \pm 63$

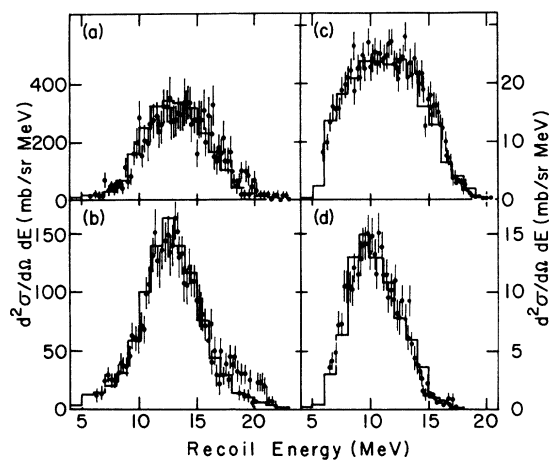


FIG. 3. Experimental (points) and calculated (histograms) laboratory double-differential cross sections of heavy residual nuclei ranging from Ne to Si formed in the reaction 22.48 MeV  $^{18}\text{O}$  on  $^{12}\text{C}$ . Statistical counting uncertainties are shown for the experimental points. The laboratory angles and the element which the energy scale refer to are as follows: (a)  $6^\circ$ , Al/Si (average between Al and Si); (b)  $10^\circ$ , Al; (c)  $17^\circ$ , Mg; (d)  $21^\circ$ , Mg.

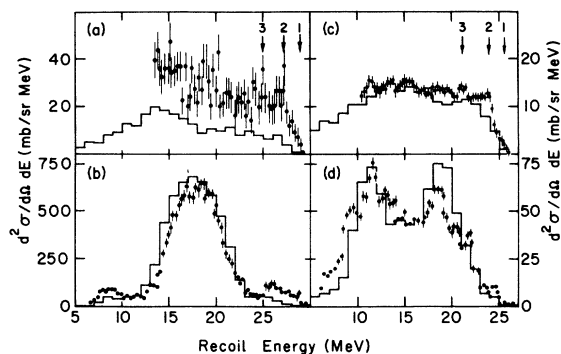


FIG. 4. Experimental (points) and calculated (histograms) laboratory double-differential cross sections of heavy residual nuclei formed in the reaction 32.63 MeV  $^{16}\text{O}$  on  $^{12}\text{C}$ . Statistical counting uncertainties are shown for the experimental points. The residual nuclei, the laboratory angles, and the elements which the energy scales refer to are as follows: (a)  $^{20}\text{Ne}$  at  $7^\circ$ , Ne; (b) Na-Si at  $7^\circ$  (cross sections below 14.7 MeV include the  $^{20}\text{Ne}$  yield), Mg/Al; (c)  $^{20}\text{Ne}$  at  $15^\circ$ , Ne; (d) Na-Si at  $15^\circ$  (cross sections below 10.9 MeV include the  $^{20}\text{Ne}$  yield), Na/Mg. The arrows in sections (a) and (c) indicate recoil energies of  $^{20}\text{Ne}$  corresponding to the following transitions of the reaction  $^{12}\text{C}(^{16}\text{O}, ^{20}\text{Ne})^8\text{Be}$  g.s.: (1)  $^{20}\text{Ne}$  (g.s.); (2)  $^{20}\text{Ne}$ (1<sup>st</sup>, 1.63 MeV); (3)  $^{20}\text{Ne}$  (2<sup>nd</sup>, 4.25 MeV).

number) calibration curves were used as indicated in the figure captions. Some measured differential cross sections of heavy residual nuclei are displayed in Figs. 5 and 6. By integration of the differential cross sections over angle, the total complete fusion cross section was obtained. The values of the measured complete fusion cross sections are presented in Table I. The contribution of the angular region  $0^\circ$ – $4^\circ$  lab to the fusion cross section was estimated by the extrapolation of experimental angular distributions as described in Sec. IV. The errors associated with the extrapolation were estimated from the quality of the agreement between experiment and calculations over the entire angular range. It is important to note that the contribution of the unmeasured portion of the angular distribution to the total fusion cross section is not more than approximately 10%.

The fusion cross sections of the reaction  $^{16}\text{O} + ^{12}\text{C}$  at 7 and 8 MeV c.m. agree within the experimental uncertainties with the combined cross sections of evaporated light particles measured previously for the same reaction.<sup>3,4</sup> The latter experiments involved the measurement of protons and  $\alpha$  particles,<sup>3</sup> as well as of  $^{27}\text{Si}$ , indicative of neutron emission.<sup>4</sup> For the excitation energies which correspond to the above mentioned kinetic energies, the contribution to the yield from two- (or more) particle decays is expected to be small.

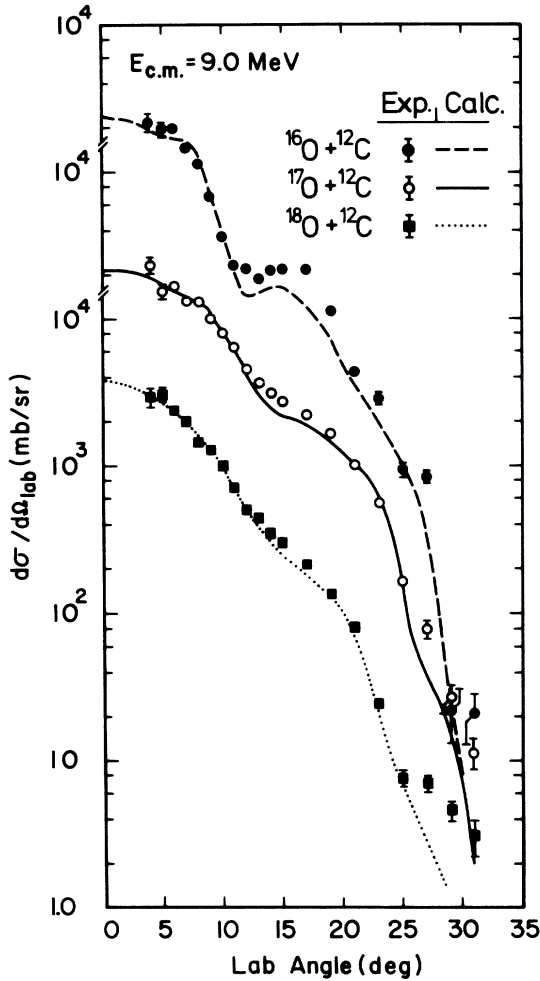


FIG. 5. Measured (points) and calculated (curves) laboratory angular distributions of heavy evaporation residues at 9 MeV c.m.

#### IV. DISCUSSION

The formation of all elements listed in Fig. 1 has been observed in the present experiment. In some of the spectra individual isotopes are identified unambiguously because of large differences between reaction  $Q$  values or from two-body kinematics. Of particular interest are the relatively large  $^{20}\text{Ne}$  cross sections in the reaction  $^{16}\text{O} + ^{12}\text{C}$  as well as the formation of neon in the bombardments of  $^{12}\text{C}$  with  $^{17}\text{O}$  and  $^{18}\text{O}$ . Here possible contributions from  $\alpha$ -transfer processes should be considered. A few comments about these reactions will be added later.

Since many excited states are involved in the evaporation, the heavy residual nuclei are expected to possess broad and rather smooth energy spectra. This feature is clearly observed in Figs. 3 and 4.

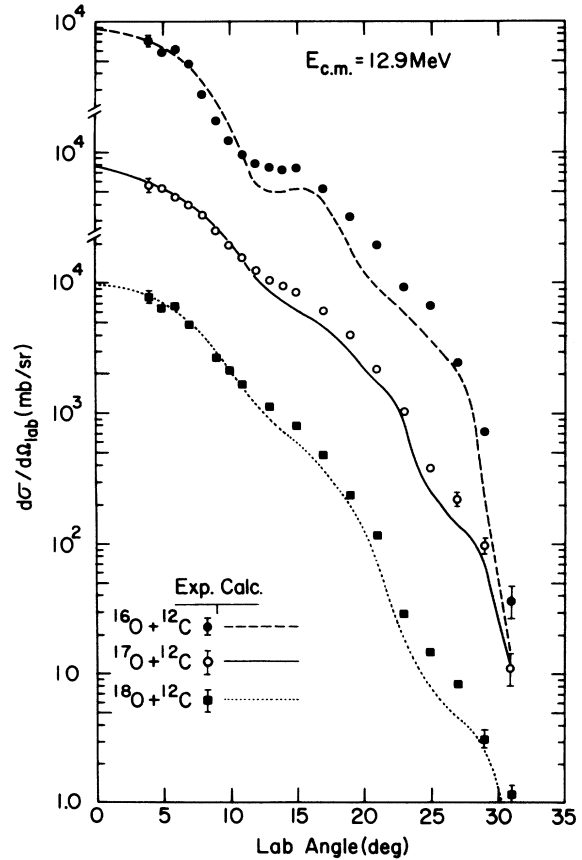


FIG. 6. Measured (points) and calculated (curves) laboratory angular distributions of heavy evaporation residues at 12.9 MeV c.m.

A quantitative analysis of the decay has been carried out within the framework of the statistical model, assuming that a complete equilibration of the excitation energy is reached among the constituents of the silicon composite system. It was further assumed that the evaporated particles are emitted isotropically in the center-of-mass frame. The latter assumption enables one to perform practical calculations, particularly when two or more particles are emitted sequentially.

The evaporation calculations have been performed with an improved version of the Dostrovsky, Fraenkel, and Friedlander (DFF) evaporation<sup>5,6</sup> code. In the calculations we considered the emission of the following particles:  $n$ ,  $p$ ,  $d$ ,  $t$ ,  $^3\text{He}$ , and  $\alpha$ . Emission probabilities were calculated according to the procedure described in Ref. 6. All known discrete low-lying levels were taken into account. Inverse light particle cross sections<sup>5</sup> were readjusted in order to obtain better agreement with optical model predictions. A complete list of the parameters will be presented elsewhere.<sup>7</sup>

A visual display of the calculated angular distri-

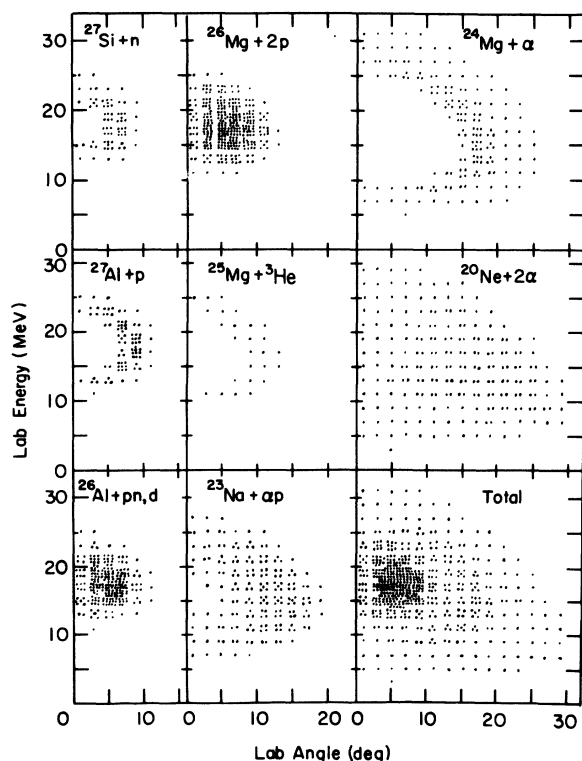


FIG. 7. Calculated yield as function of energy and angle of heavy residual nuclei for 50 000 evaporation cascades in the reaction 32.63 MeV  $^{16}\text{O}$  on  $^{12}\text{C}$ . The events were summed over energy intervals of 2 Mev and angular intervals of  $2^\circ$  in the laboratory. The section marked "Total" represents the combined yield. Each dot represents 1–100 events in the "Total" section and 1–50 events in all others.

butions and energy spectra obtained for the reaction 32.63 MeV  $^{16}\text{O}$  with  $^{12}\text{C}$  is presented in Fig. 7. Events were summed over energy intervals of 2 MeV and angular intervals of  $2^\circ$  in the laboratory. Similar calculations have also been performed for all other bombardments. Computed energy spectra have been used to correct the measured yield for its small unmeasured fractions. Computed double-differential cross sections are presented as histograms in Figs. 3 and 4. The angular "resolution" of the calculations was chosen to be  $2^\circ$  in the laboratory. In addition, events were summed over intervals of 1 MeV. In the calculations presented in Figs. 3 and 4, the statistical uncertainties are about the same or better than the statistical uncertainties associated with the experimental data.

Calculated angular distributions of fusion residues are presented as curves in Figs. 5 and 6. Since the calculations provide only relative differential cross sections, the absolute scales of the calculated cross sections were determined by weighted least-square fits to the experimental data.

The calculated results were then used in extrapolating the experimental differential cross sections to the angular region  $0^\circ$ – $4^\circ$  lab as described above. Some of the details of the energy spectra and those of the angular distributions may be understood with the aid of Fig. 7. Firstly, differences are expected between energy spectra of heavy residues formed in one-particle evaporation and those of products formed in two- (or more) particle emission. These differences are easily explained by simple kinematic considerations. Secondly, large differences are expected between maximum recoil angles and recoil energies obtained in  $\alpha$  particle emission and those obtained in nucleon emission. Thus, a maximum recoil angle of approximately  $12^\circ$  lab is predicted for heavy residual nuclei formed by  $n$ ,  $p$ ,  $2n$ ,  $np$ , and  $2p$  evaporation. Shoulders at approximately  $12^\circ$  lab appear, indeed, in the measured angular distributions (Figs. 5 and 6), coinciding with the disappearance of Si and Al in the spectra. The shapes as well as the structures in the measured angular distributions are reproduced well by the calculations.

The agreement of the calculations with the shapes of the energy spectra is also generally good. Some of the discrepancies, observed mainly for the reaction  $^{16}\text{O} + ^{12}\text{C}$ , may be attributed to the use of approximate energy scales for the display of the experimental results, and the poorer angular resolution of the calculations ( $2^\circ$  lab as compared with  $0.3^\circ$  in the experiment).

Due to the insufficient resolution of individual products, it is difficult to test quantitatively the agreement between the calculations and experiment as to the relative yields of the heavy evaporation residues. For the reaction  $^{16}\text{O} + ^{12}\text{C}$  the yield of  $^{20}\text{Ne}$  is underestimated (Fig. 4). This discrepancy may be explained in part by the neglect of angular momentum effects in the calculations. Comments on the importance of angular momentum effects in low energy heavy-ion reactions can be found, for example, in Refs. 8 and 9.

As mentioned above, the shapes of the energy spectra in Fig. 4 indicate that the formation of  $^{20}\text{Ne}$  in the reaction  $^{16}\text{O} + ^{12}\text{C}$  proceeds predominantly via the compound nucleus mechanism  $^{12}\text{C}(^{16}\text{O}, 2\alpha)^{20}\text{Ne}$ . Only small contributions (less than 1% of the fusion cross section at 14 MeV c.m.) of the  $\alpha$ -transfer reaction  $^{12}\text{C}(^{16}\text{O}, ^{20}\text{Ne})^8\text{Be}$  are observed in the form of small peaks in the energy spectra of Figs. 4(a) and 4(c). This reaction includes transitions to  $^{20}\text{Ne}(g.s., 0^+)$ ,  $^{20}\text{Ne}(1st, 1.63 \text{ MeV}, 2^+)$ , and  $^{20}\text{Ne}(2nd, 4.25 \text{ MeV}, 4^+)$ . The same transitions have been observed by Gutbrod<sup>10</sup> at 65 MeV lab. Analysis by Yoshida<sup>11</sup> has shown that the data<sup>10</sup> are indeed consistent with a direct  $\alpha$ -transfer process. It should be noted that the formation of other neon

TABLE II. Fusion barrier parameters. The energy range of the measurements relative to the barrier height is indicated. The quantity  $r_b$  is the barrier distance radius parameter defined by  $r_b = R_b / (A_1^{1/3} + A_2^{1/3})$ , and  $\Delta E_b$  is the percentage reduction of the barrier height relative to  $^{16}\text{O} + ^{12}\text{C}$ . Best reduced  $\chi^2$  values are quoted ( $f=4$ ).

Reaction	Energy range	$E_b$ (MeV)	$\hbar\omega_b$ (MeV)	$R_b$ (fm)	$r_b$ (fm)	$\Delta E_b$ (%)	$\chi^2/f$
$^{16}\text{O} + ^{12}\text{C}$	0.88–1.76	$7.94 \pm 0.15$	$2.91 \pm 0.36$	$7.23 \pm 0.24$	$1.50 \pm 0.05$		0.58
$^{17}\text{O} + ^{12}\text{C}$	0.91–1.82	$7.68 \pm 0.12$	$2.62 \pm 0.33$	$7.27 \pm 0.20$	$1.50 \pm 0.04$	$3.2 \pm 2.4$	0.21
$^{18}\text{O} + ^{12}\text{C}$	0.93–1.86	$7.55 \pm 0.11$	$2.63 \pm 0.31$	$7.45 \pm 0.20$	$1.52 \pm 0.04$	$4.9 \pm 2.3$	0.16

isotopes in the compound nucleus reaction  $^{16}\text{O} + ^{12}\text{C}$  is energetically excluded or highly unfavored from phase-space considerations. The formation of neon in the bombardments with  $^{17}\text{O}$  and  $^{18}\text{O}$  is explained by the reactions  $^{12}\text{C}(^{17}\text{O}, 2\alpha)^{21}\text{Ne}$  and  $^{12}\text{C}(^{18}\text{O}, 2\alpha)^{22}\text{Ne}$ .

Inspection of Table I reveals marked differences between the three complete fusion excitation functions. At 14 MeV c.m. the fusion cross sections of the three reactions are essentially the same. However, at 7 MeV c.m. the fusion cross section of the reaction  $^{18}\text{O} + ^{12}\text{C}$  is larger by a factor of  $1.9 \pm 0.4$  than that of the reaction  $^{16}\text{O} + ^{12}\text{C}$ . The cross sections of the reaction  $^{17}\text{O} + ^{12}\text{C}$  are intermediate.

A systematic analysis of the data has been performed according to the strong absorption model, using the formalism of Wong.<sup>12</sup> This approach is justified here since absorption leads predominant-

ly to fusion.<sup>2,9,13</sup> Therefore the characteristics of the fusion barrier may be determined from simple barrier penetrability considerations. According to Wong<sup>12</sup> the fusion cross section may be written as

$$\sigma(E) = \pi \kappa^2 \sum_l (2l+1) P(l, E), \quad (1)$$

where  $P(l, E)$  is the penetrability probability of the partial wave  $l$ . The sequence of barriers is approximated by parabolas with heights

$$E_l = E_b + \hbar^2 l(l+1)/2\mu R_b^2, \quad (2)$$

and with a constant curvature  $\hbar\omega_b$ . In Eq. (2) the quantity  $E_b$  is the height of the  $s$ -wave barrier and  $R_b$  is the distance between the centers of the two interacting nuclei at the barrier. With these approximations the penetrability is given by the Hill-Wheeler formula<sup>14</sup>

$$P(l, E) = \{1 + \exp[2\pi(E_l - E)/\hbar\omega_b]\}^{-1}. \quad (3)$$

The barrier characteristics which have been obtained by three-parameter least  $\chi^2$  fits<sup>15</sup> to the data are listed in Table II. The errors associated with the parameters pertain to the goodness of fit and include the effect of the experimental errors. The corresponding calculated excitation functions are compared with experimental cross sections in Fig. 8. It can be seen in Table II that the curvatures of the three barriers are very close to one another. The distances  $R_b$  follow essentially the  $A_1^{1/3} + A_2^{1/3}$  law. A systematic decrease in the barrier height with increasing  $R_b$  is clearly observed. The first two features are different from those observed by Scobel *et al.*<sup>16</sup> for the systems  $^{35}\text{Cl}$  with Ni isotopes.

While the absolute values of the parameters extracted in the analysis may certainly be model dependent, it is apparent that the trends observed in Table II may be closely related to the geometrical properties of the projectiles. An estimate of the sensitivity of the barrier height to a change in the nuclear radius can be made if the Coulomb potential and the nuclear potential are treated separately. For each of the nuclei involved the barrier is far outside of the rms radius of the charge distri-

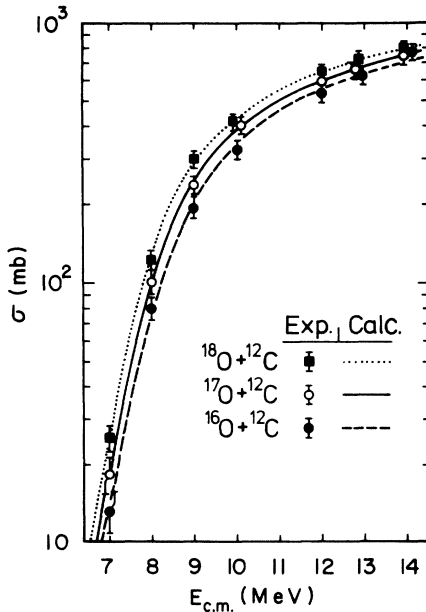


FIG. 8. Measured (points) and calculated (curves) complete fusion cross sections. (Some of the data points are slightly shifted horizontally for the sake of clarity of the figure).

bution.<sup>17</sup> The Coulomb potential at the barrier region is expected, therefore, to be very similar for the three systems, and may be well approximated by the  $1/r$  law. For a square-well nuclear potential with a range proportional to  $A_1^{1/3} + A_2^{1/3}$ , a 2% reduction in the barrier height of  $^{18}\text{O} + ^{12}\text{C}$  relative to the barrier height of  $^{16}\text{O} + ^{12}\text{C}$  is expected. This reduction is somewhat smaller than the observed reduction ( $4.9 \pm 2.3$ )%. However, the effect of the finite nuclear diffuseness cannot be neglected. According to the parameters of Table II, the size of the nuclear potential at the barrier amounts to approximately 20% of the barrier height. It is therefore evident that even a small change in the boundary diffuseness may affect the height of the fusion barrier. The results obtained in the present analysis appear to be consistent with a gradual increase in the surface diffuseness from  $^{16}\text{O}$  to  $^{18}\text{O}$ . This conclusion is in agreement with the observations of Goldring *et al.*<sup>18</sup> of the elastic scattering of  $^{16}\text{O}$ ,  $^{17}\text{O}$ , and  $^{18}\text{O}$  by  $^{12}\text{C}$ . Their phenomenological analysis has shown a systematic increase in the diffuseness with increasing neutron number.

#### V. SUMMARY AND CONCLUSIONS

The main emphasis of the present investigation centered on the experimental determination of the fusion cross sections and the recoil properties of the heavy residual nuclei formed in the bombardments of  $^{12}\text{C}$  with  $^{16}\text{O}$ ,  $^{17}\text{O}$ , and  $^{18}\text{O}$  beams. It has been shown that the formation of Ne, Na, Mg, Al, and Si isotopes is associated mainly with a statistical decay of an excited silicon composite system, formed in the fusion of projectile and target. Only a small contribution to the yield of  $^{20}\text{Ne}$  in the reaction  $^{16}\text{O} + ^{12}\text{C}$  is made by a direct process, the  $\alpha$ -transfer reaction  $^{12}\text{C}(^{16}\text{O}, ^{20}\text{Ne})^6\text{Be}$ . The differential yields of the heavy residual nuclei, as well as their energy spectra, have been reproduced rather well by the calculations. It may be concluded therefore that the assumption of the isotropic evaporation of light particles in the center-of-mass frame is adequate in reproducing recoil properties of heavy residual nuclei in the laboratory frame at

low bombarding energies.

It is of interest to note that similar investigations of recoil properties of heavy residual nuclei may be of importance not only in compound nucleus reactions but also in other reactions in which highly excited nuclei are formed. In particular, the effects of decay via particle emission on the final mass, energy, and angular distributions of products must be taken into account. Reactions in which highly excited nuclei are formed include heavy-ion deep inelastic collisions which are presently under intensive investigations at many laboratories.<sup>19</sup>

The complete-fusion cross sections of the systems oxygen with carbon are seen to differ considerably for the three reactions at low bombarding energies. It has been shown that these differences are closely related to the differences in the nuclear size and surface diffuseness of the oxygen isotopes. The effect of a larger nuclear size and/or larger diffuseness is to lower the height of the fusion barrier, if the Coulomb potential is held constant. A relatively strong dependence of the fusion barrier on the spatial distributions of the interacting nuclei is believed to be a typical feature of low energy heavy-ion reactions. Low energy heavy-ion fusion reactions may provide, therefore, an additional useful tool to probe the nuclear surface.

In view of the significant increase of the fusion cross section ratios  $\sigma(^{17,18}\text{O} + ^{12}\text{C})/\sigma(^{16}\text{O} + ^{12}\text{C})$  with decreasing beam energy, it would be of interest to study the reactions  $^{17}\text{O} + ^{12}\text{C}$  and  $^{18}\text{O} + ^{12}\text{C}$  at very low energies, in order to check their possible role in astrophysical processes. The reaction  $^{16}\text{O} + ^{12}\text{C}$  has already been shown to be of importance at certain stages of nuclear burning in stars.<sup>3,20</sup> Neutrons and  $^{28}\text{Si}$  are prominent primary decay products of the reactions  $^{17}\text{O} + ^{12}\text{C}$  and  $^{18}\text{O} + ^{12}\text{C}$ . This is not true for the reaction  $^{16}\text{O} + ^{12}\text{C}$ . Thus, very large cross sections for the former two reactions relative to those of the reaction  $^{16}\text{O} + ^{12}\text{C}$  may compensate somewhat for the low abundances of  $^{17}\text{O}$  and  $^{18}\text{O}$  at the stage of oxygen-carbon burning.

\*Present address: Nuclear Structure Laboratory, University of Rochester, Rochester, New York.

†Present address: Division of Physics, National Research Council of Canada, Ottawa, Canada.

<sup>1</sup>M. G. Mazarakis and W. E. Stephens, *Phys. Rev. C* **7**, 1280 (1973); J. R. Patterson, H. Winkler, and C. S. Zaidins, *Astrophys. J.* **157**, 367 (1969).

<sup>2</sup>J. A. Kuehner and E. Almqvist, *Phys. Rev.* **134**, B1229 (1964).

<sup>3</sup>J. R. Patterson, B. N. Magorcka, G. D. Symons, and N. M. Zuk, *Nucl. Phys.* **A165**, 545 (1971).

<sup>4</sup>H. Spinka and H. Winkler, *Nucl. Phys.* **A223**, 456 (1974).

<sup>5</sup>I. Dostrovsky, Z. Fraenkel, and G. Friedlander, *Phys. Rev.* **116**, 683 (1959).

<sup>6</sup>Y. Eyal, M. Beckerman, and H. H. Gutbrod, *Nucl. Phys.* **A221**, 119 (1974).

<sup>7</sup>M. Beckerman and Y. Eyal, (unpublished).

<sup>8</sup>W. R. Falk, A. Huber, U. Matter, R. W. Benjamin, and P. Marmier, *Nucl. Phys.* **A140**, 548 (1970).

<sup>9</sup>Y. Eyal, I. Dostrovsky, and Z. Fraenkel, *Nucl. Phys.* **A179**, 594 (1972).

<sup>10</sup>H. H. Gutbrod, Ph.D. thesis, Heidelberg, 1970 (unpub-)

lished).

<sup>11</sup>H. Yoshida, *Phys. Lett.* **47B**, 411 (1973).

<sup>12</sup>C. Y. Wong, *Phys. Rev. Lett.* **31**, 766 (1973).

<sup>13</sup>In a recent study of inelastic scattering and several particle-transfer channels in the reactions  $^{17}\text{O} + ^{12}\text{C}$  and  $^{18}\text{O} + ^{12}\text{C}$  at 12.9 and 14 MeV c.m. it was found that the total nonfusion cross sections do not exceed more than a few percent of the fusion cross sections reported in this work. (See also R. Chechik, H. Stocker, Y. Eyal, and Z. Fraenkel, in *Proceedings of the International Conference on Reactions between Complex Nuclei, Nashville, Tennessee, 1974*, edited by R. L. Robinson *et al.* (North-Holland, Amsterdam/American Elsevier, New York, 1974), Vol. I, p. 6.

<sup>14</sup>D. L. Hill and J. A. Wheeler, *Phys. Rev.* **89**, 1102

(1953).

<sup>15</sup>In this analysis the nucleus  $^{17}\text{O}$  was treated as a spinless particle.

<sup>16</sup>W. Scobel, A. Mignerey, M. Blann, and H. H. Gutbrod, *Phys. Rev. C* **11**, 1701 (1975).

<sup>17</sup>R. P. Singhal, J. K. Moreira, and H. S. Caplan, *Phys. Rev. Lett.* **24**, 73 (1970).

<sup>18</sup>G. Goldring, H. M. Loebenstein, I. Plessner, and M. W. Sachs, *Phys. Lett.* **25B**, 538 (1967).

<sup>19</sup>See, for example, B. Gatty, D. Guerreau, M. Lefort, J. Pouthas, X. Tarrago, J. Galin, B. Cauvin, J. Girard, and H. Nifenecker, *J. Phys. (Paris) Lett.* **35**, L117 (1974), and references therein.

<sup>20</sup>S. E. Woosley, W. D. Arnett, and D. D. Clayton, *Astrophys. J. Suppl.* **26**, 231 (1973), and references therein.